2A.1 TROPICAL CYCLONE-INDUCED THERMOCLINE WARMING AND ITS REGIONAL AND GLOBAL IMPACTS

Michael R. Bueti *, Isaac Ginis, Lewis M. Rothstein
University of Rhode Island – Graduate School of Oceanography, Narragansett, RI

1. INTRODUCTION

Tropical cyclones (TCs) are highly coherent, intermittent, and intense wind and precipitation events, notable for their ability to induce strong vertical ocean mixing over the course of their lifetime. Strong seas surface temperature (SST) cooling associated with TC passage over the ocean produces a well-understood cold wake due to vertical mixing of mixed layer and upper thermocline waters (Price, 1981), and anomalous surface buoyancy fluxes and upwelling induced by the strong wind stress curl.

Emanuel (2001) estimated that the restoration of an idealized cold wake could result in the introduction of up to $5{\cdot}10^{21}$ J of anomalous ocean heat uptake (OHU), with an idealized modeling study producing an annual mean OHU rate of 1.4±0.7 PW, with up to 1/3 of this heating carried poleward as part of the Atlantic meridional overturning circulation on decadal timescales.

Subsequent studies have attempted to refine these estimates, based on use of remote sensing measurements, in situ observations, and numerical simulations. Global OHU rates ranged from 0.15 PW when accounting for seasonal effects (Jansen et al, 2010) to 0.34 PW from ARGO float data (Cheng et al., in review). Ocean model responses TC forcing have notable sensitivities to model resolution, temporal, and spatial distribution of (Kaufman et al, in prep; Manucharyan et al, 2011; Jansen and Ferrari, 2009).

We expand on previous studies of this topic using a global mesoscale eddy permitting ocean-ice general circulation model with realistic TC surface boundary conditions. In this way, we hope to better understand the rate and magnitude of TC induced OHU over intraseasonal and interseasonal timescales, both globally and in the individual ocean basins.

2. METHODS

2.1 *The Ocean Model*

We use GFDL's Modular Ocean Model (MOM), version 4 (Griffies, 2009). MOM is a hydrostatic primitive equation ocean model configured using a Boussinesq approximation with a free surface algorithm and coupled to the Sea Ice Simulator ice model to handle processes in the high latitudes. We use an ocean-ice configuration with eddy-permitting resolution taken from the CM2.5 coupled climate model documented in Delworth et al. (2012). The horizontal resolution varies from 28 km at the equator to 8-11 km at high latitudes. The model has 50 vertical levels, 24 of which are in the upper 500 m of the ocean.

Vertical mixing of tracers and momentum is handled by the KPP boundary layer scheme (Large et al., 1994), which computes enhanced mixing with a boundary layer depth determined according to a bulk Richardson number. MOM parameterizes the effect of sub-mesoscale mixed layer eddies according to Fox-Kemper et al. (2011), with these eddies enhancing the ventilation of TC warm anomalies (Jansen et al., 2010).

2.2 *Air-Sea Fluxes and TC Forcing*

The ocean model is forced with air-sea boundary conditions as in the CORE-II experiments described by Griffies et al. (2009). 10m winds (U_{10}) are provided every six hours on a 1° resolution grid. The CORE-II winds are relatively coarse, so that TC winds are poorly resolved if present at all (Fig. 1a).

In this study we introduce two changes to the CORE-II boundary conditions. First, the parameterization of the drag coefficient, C_D, is modified for strong winds. For U_{10}>12.5 m s^{-1} we replace the linear Large and Yeager (2004) parameterization with the formulation of Moon et al. (2007), empirically derived from coupled wave-wind model simulations in hurricanes. This hybrid drag coefficient increases more slowly and levels off for U_{10}>40 m s^{-1}.

Second, we modify the CORE-II winds by introducing synthetic TCs based on the NHC and JTWC TCVitals database. We use intensity and structure data from TCVitals, specifically radius of maximum wind, maximum wind speed, radius of outermost closed isobar, and the radii of the 18 m s^{-1} and 26 m s^{-1} winds. Based on these parameters, an asymmetric synthetic wind field is generated for each storm in the TCVitals, as is done for operational forecasting (Bender et al. 2007), which is then embedded into the CORE-II winds (Fig. 1b). For times when extended structure data is unavailable, we instead use the axisymmetric wind speed profile of Holland (1980).

2.3 *Experimental Procedure*

The model is run from 1 June 2004-31 May 2005 in two forcing configurations. The "control experiment" has surface winds based only on the CORE-II forcing. The "TC experiment" uses CORE-II winds augmented by embedding the synthetic TCs. An "anomaly" will be defined as the difference between the ocean realizations in the TC and control experiments, thus yielding the net thermal and dynamical effects of TC activity. Ocean initial temperature and salinity fields are derived from GFDL's Ocean Data Assimilation

* *Corresponding author address:* Michael R. Bueti, University of Rhode Island, Graduate School of - Oceanography, 215 South Ferry Road, Narragansett, RI 02882; e-mail: mbueti@my.uri.edu.

Experiment product (Zhang et al., 2007), with the model spun up for six months prior to simulating the TC impact.

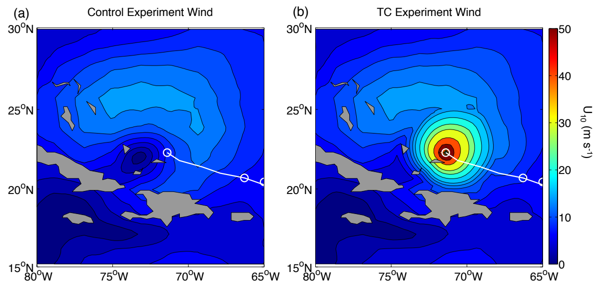

Fig. 1: 10m wind speed magnitude during Hurricane Frances (1 September 2004) from the control experiment (a) and with the embedded TC (b).

3. RESULTS

3.1 *Global and Basin Ocean Temperature Response*

Fig. 2 and 3 show the 1 October 2004 temperature and temperature anomaly fields at the ocean surface, and at the 98.7m depth level. Strong cold wakes of recent TCs are present at the surface in the West Pacific, East Pacific, and North Atlantic.

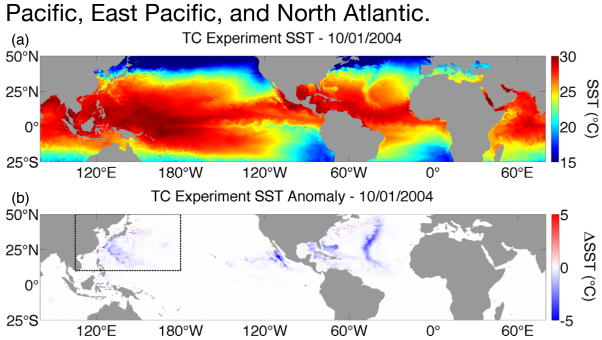

Fig. 2: Global SST (a) and anomaly (b) fields, demonstrating recent and recovering TC cold wakes in the North Atlantic, West Pacific, and East Pacific on 1 October 2004.

Warming from mixing and downwelling of mixed layer water and downwelling is present and persistent at depth throughout the TC forced regions (Fig. 3). Cooling from upward Ekman pumping is present as well, offsetting the warming from downwelling. On average, the temperature anomaly field at depth is dominated by warming.

The laterally averaged temperature anomaly is shown in Fig. 4 globally and for individual ocean basins, near the peak of northern TC activity (1 October 2004) and after one year of model integration (31 May 2005).

The West Pacific, East Pacific, and North Atlantic have cooling on 1 October down to ~50m, 30m, and 40m respectively (Fig. 4b,c,d). West Pacific warming has a deeper and broader peak than either the North Atlantic or East Pacific, while the East Pacific warming is both the shallowest and weakest. This variability is due to differences in the TC forcing and local stratification.

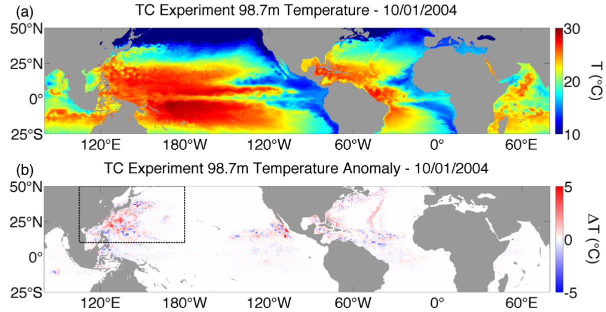

Fig. 3: Global temperature (a) and anomaly (b) fields at the 98.7m depth level, demonstrating the mixing induced warming at depth, as well as warming and cooling from dynamical effects in the North Atlantic, West Pacific, and East Pacific on 1 October 2004.

Cooling in the North Atlantic has vanished by 31 May, with a weaker and deeper warm anomaly centered around 100m. The East Pacific warm anomaly on 31 May is nearly as strong as that on 1 October, and has deepened by ~60m. The West Pacific has two peaks of weaker persistent warming, one shallower (~50m) and the other deeper (~160m) than on 1 October.

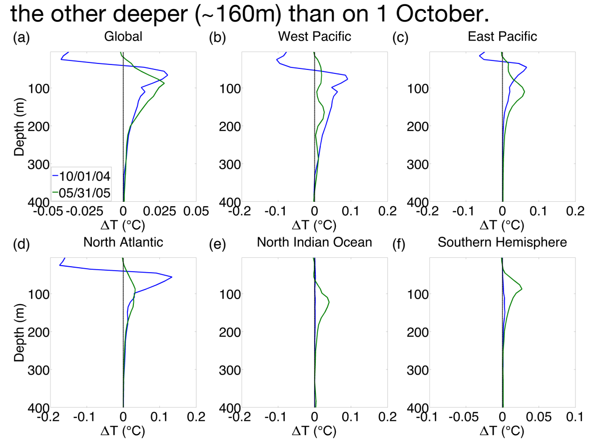

Fig. 4: Global and basin averaged temperature anomaly profiles at the peak of northern TC activity (1 October 2004) and on 31 May 2005.

The North Indian Ocean, consistent with its weakened and offset TC season has nearly zero subsurface accumulation on 1 October, while by 31 May there is a strong warming centered on 110m (Fig. 4e). In the Southern Hemisphere (Fig. 4f) there is weak warming at depth on 1 October, centered on 150m, which we do not attribute to direct TC forcing as this is prior to the start of austral TC activity. By 31 May there is a sharp warming centered on 95m. The origin of this deep anomalous heating at times and locations removed from TC induced mixing, the bifurcated West Pacific warming on 31 May, and the strong and deepened East Pacific warming are explored in Section 3.4.

3.2 *Ocean Heat Uptake*

The upper ocean heat content (OHC) and anomaly (ΔOHC) are defined to quantify the bulk thermal impact of TC mixing on the ocean.

$$OHC(t) = c_p\rho_o \int_{-729\,m}^{0\,m} dz \int_{x_w}^{x_e} dx \int_{y_s}^{y_n} dy \Delta T_{729\,m} \quad (1a)$$

$$\Delta T_{729\,m} = T(x,y,z,t) - T(x,y,z=729\,m,t) \quad (1b)$$

$$\Delta OHC(T) = OHC_{TC}(t) - OHC_{con}(t) \quad (1c)$$

where c_p is the heat capacity of seawater, ρ_o is the Boussinesq seawater density, and the subscripts "TC" and "con" denote results from the TC and Control experiments.

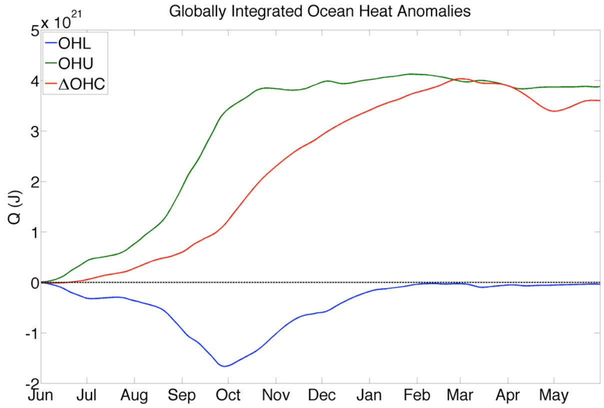

Fig. 5: Time series of the globally integrated OHL, OHU, and ΔOHC from 1 June 2004-31 May 2005.

Ocean heat loss (OHL) and ocean heat uptake (OHU) decompose the head content anomaly into shallow cooling and deep warming constituents

$$OHL(t) = c_p\rho_o \int_{z_1}^{0\,m} dz \int_{x_w}^{x_e} dx \int_{y_s}^{y_n} dy \Delta T(x,y,z,t) \quad (2a)$$

$$OHU(t) = c_p\rho_o \int_{z_2}^{z_2} dz \int_{x_w}^{x_e} dx \int_{y_s}^{y_n} dy \Delta T(x,y,z,t) \quad (2b)$$

where $\Delta T(x,y,z,t) = T_{TC}(x,y,z,t) - T_{con}(x,y,z,t)$. These integrals are first carried out horizontally, to obtain a heat anomaly profile with clear zero crossings, as in Fig. 4. OHL is integrated from the surface to the first zero crossing (z_1) and OHU from the first zero crossing until the second zero crossing or, if one is not present, the warm anomaly has attenuated to 1% of its peak value (z_2).

Time series of OHL, OHU, and ΔOHC are integrated globally from 1 June 2004-31 May 2005 (Fig. 5). OHL increases slowly before accelerating with increased storm activity in August, peaking at $1.7 \cdot 10^{21}$ J. Global OHL subsequently decays until there is none remaining by February, indicating an average restoration of the climatological mixed layer (CML). OHU temporal structure mirrors that of OHL through October, with anomalous heating increasing through August before leveling off at $4.1 \cdot 10^{21}$ J. OHU continues to increase slowly through January, before decreasing slightly to a 31 May value of $3.9 \cdot 10^{21}$ J. ΔOHC lags OHU, with the difference between the two equivalent to the OHL. February ΔOHC is comparable to OHU, by which time the CML is restored, giving confidence that OHU is in fact capturing the warming anomaly in an average sense.

Fig. 6a shows the basin OHL. The strongest cooling is seen in the North Atlantic and West Pacific. While its peak is lower, West Pacific OHL is broader, consistent with the longer typhoon season. The East Pacific and Southern Hemisphere have weaker OHL, peaking in late September and mid-April respectively, consistent with the timing and duration of direct TC forcing in those regions.

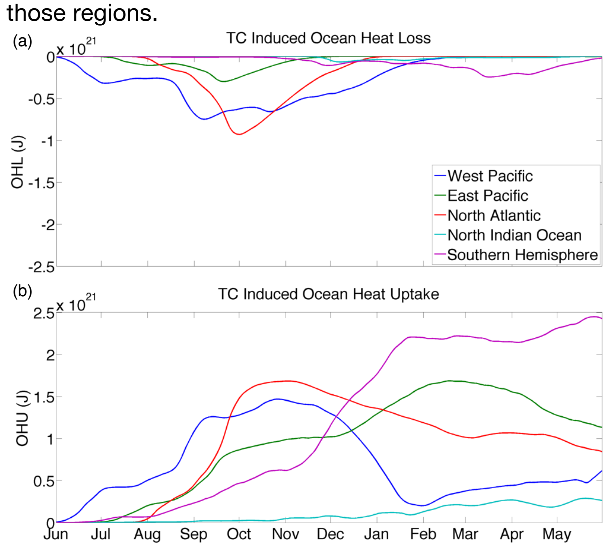

Fig. 6: Time series of OHL (a) and OHU (b) integrated over the individual ocean basins from 1 June 2004-31 May 2005.

Basin integrated OHU is shown in Fig. 6b. Initial heat uptake follows the structure of the local OHL, as with Global OHU. North Atlantic OHU peaks in early October before gradually falling by 50% by 31 May 2005. West Pacific OHU peaks in early November, at a lower value than the North Atlantic peak despite the greater local TC forcing. OHU in the West Pacific decreases rapidly between November and March, with less than 1/3 of the maximum heating remaining on 31 May.

In contrast, East Pacific OHU peaks at $6 \cdot 10^{20}$ J, and subsequently increases by ~1/3 after the conclusion of local TC activity. OHU in the Southern Hemisphere begins to accumulate during the northern summer, increasing rapidly in November before leveling off in February. There is a slight decrease in Southern Hemisphere OHU in March, followed by an increase that corresponds with local TC activity. The North Indian Ocean sees a small accumulation through the course of the northern winter.

The striking behavior of West Pacific, East Pacific, and Southern Hemisphere TC induced OHU bears deeper analysis, specifically the reasons for their apparently compensatory variability. The heat anomaly budget for the region delineated by the dashed box in Fig. 2b and 3b is calculated (Fig. 7) to understand the reasons for the drastic drop in West Pacific OHU. Accumulated anomalous heating through the ocean surface results in a warming of the ocean.

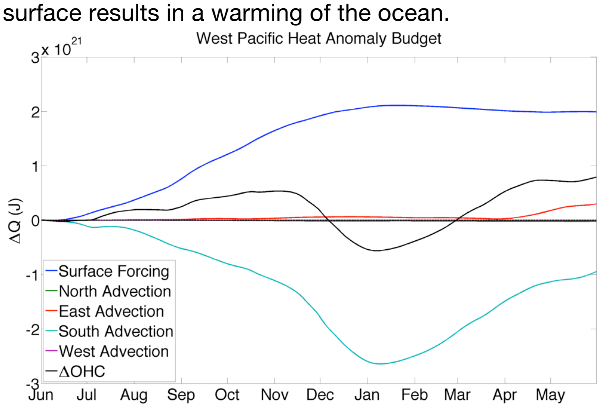

Fig. 7: Time series of the accumulated heat flux anomalies in the West Pacific TC forcing region, calculated for the domain outlined in Fig. 2b and 3b from 1 June 2004-31 May 2005. Positive values indicate an increase of heat within the control volume.

There is a strong and rapid accumulation of anomalous ocean heat transport

$$\Sigma \Delta OHT = c_p \rho_o \int_{x_w}^{x_e} dx \int_0^H \int_0^t dt' \Delta(v \cdot T) \quad (3a)$$

$$\Delta(v \cdot T) = v_{TC} \cdot T_{TC} - v_{con} \cdot T_{con} \quad (3b)$$

across the southern boundary. This southward heat export continues through January, with a peak value $2.75 \cdot 10^{21}$J before turning northward. A considerably weaker and slower zonal export of anomalous heat occurs at the eastern boundary. The surface and advective forcing are balanced by a regional change in OHC (Eq. 1c). This analysis indicates that the drop in West Pacific OHU in Fig. 6b is consistent with a redistribution of anomalous heat from the subtropical to the tropical Pacific.

3.3 *Meridional Transport*

Anomalous meridional heat export, and its convergence in the deep tropics, is clearly seen in Fig. 8, where Eq. 3a has been integrated around the globe every 10° from 30°S to 30°N, producing time series of the accumulated meridional TC induced heat transport anomaly. There is a clear southward transport in the northern hemisphere starting in late summer. This OHT anomaly strengthens between 20°N and 10°N before penetrating across the equator. By 10°S there is no further transport accumulation, confirming the convergence of heat in the equatorial region.

The temporal structure and magnitude of the global OHT anomaly accumulation across 10°N is consistent with that across the southern boundary of the West Pacific control volume analyzed in Fig. 7, establishing that the equatorial ΔOHT convergence is dominated by export of TC induced OHU out of the subtropical West Pacific. For this reason, the remainder of the analysis focuses on the West Pacific transport and circulation. While there is a significant decrease in OHU in the North Atlantic between November and May (~50%), it is not associated with export of heat to the tropical Atlantic. Rather, this decrease is likely due to the reventilation mechanism of Jansen et al. (2010).

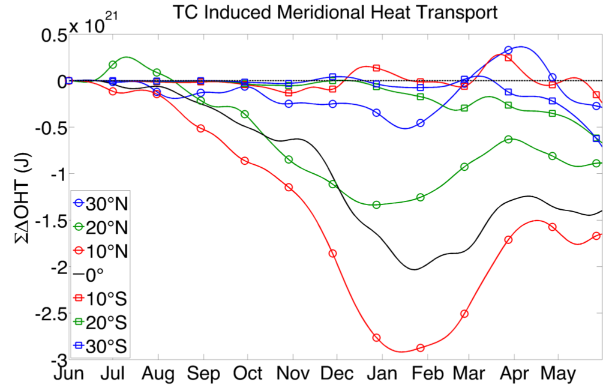

Fig. 8: Accumulated meridional heat transport anomaly across latitudinal boundaries from 1 June 2004-31 May 2005. Negative values indicate southward transport.

3.4 *Subtropical-Tropical Interaction*

The currents in the West Pacific upper-thermocline are shown in Fig. 9. Zonal and meridional currents are averaged from 56m to 253m to capture the flow field over the depths where TC mixing deposits heat. The region shown contains nearly all of the West Pacific TC activity. Zonal flow is predominantly westward, carrying TC induced heat anomalies towards the western boundary, where they enter either the Kuroshio Current to be advected poleward or the Mindanao Current to be advected into the deep tropics. Whether a water mass enters the Kuroshio or Mindanao is determined by its latitude upon reaching the western boundary and the location of the bifurcation of the North Equatorial Current (NEC).

The location of the NEC bifurcation varies seasonally, consistent with the observational findings of Qu and Lukas (2003) who hypothesized that changes in local Ekman pumping associated with monsoonal winds alter the circulation such that the bifurcation reaches its northernmost location between November and December, before migrating south through July. The bifurcation point is around 15°N between August and October (Fig. 9a), 16°N between November and January (Fig. 9b), and as far south as 12°N between

February and April (Fig. 9c). Times when the bifurcation is further to the north correspond with elevated anomalous heat transport into the tropics, with the proportion of mid-gyre waters flowing into the Mindanao elevated relative to the annual mean.

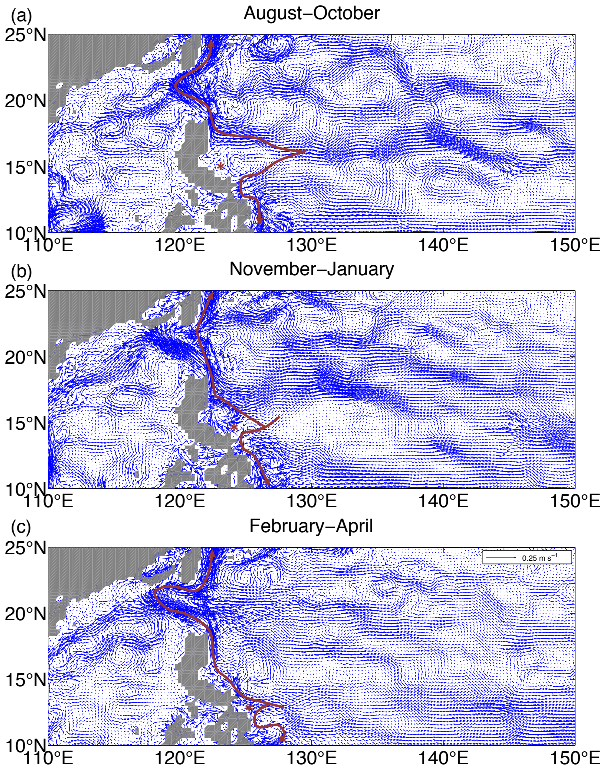

Fig. 9: Thermocline averaged currents in the West pacific during the period of peak TC forcing (a), greatest southward advection (b), and reversal (c). Red stars approximate the bifurcation of the NEC into the Kuroshio Current and Mindanao Current. Red lines are a schematic representation of water parcel trajectories into the Kuroshio and Mindanao.

Warm anomalies are advected equatorward as part of the subtropical cell (McCreary Jr and Lu, 1994). Large-scale southward deflection of the NEC between 125ºE and 130ºE in the November-January period further enhances the flow into the Mindanao, corresponding with the period of greatest ΔOHT into the tropics. The late winter period February-April sees a relaxation of the currents consistent with the reduced wind stress curl during the southwest monsoon. Meridional flow is now predominantly northward, with waters from the tropics penetrating the gyre interior and entering the Kuroshio, accounting for the seasonal reversal in ΔOHT seen in Fig. 7 and 8.

The model representation of the mean annual equatorial circulation averaged from 56m-330m is shown in Fig. 10. The rapid flow in the Mindanao is clearly displayed, feeding into the Indonesian Throughflow west of 120ºE and the Equatorial Undercurrent (EUC) east of the Philippines and eastward into the open Pacific. The MOM representation of the EUC reaches speeds exceeding 1 m s^{-1} and is sharply sloped zonally along isopycnals, consistent with observations (Griffies et al., 2009). Advection by the EUC would serve as a rapid mechanism of zonal OHU redistribution should TC induced warm anomalies reach the undercurrent.

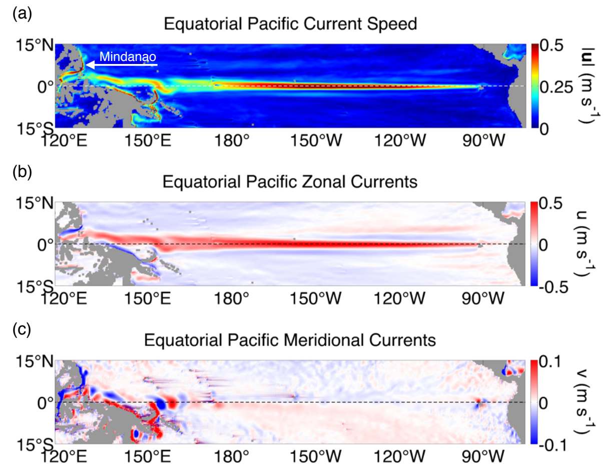

Fig. 10: Currents in the equatorial Pacific, averaged from 1 June 2004-31 May 2005 and over the 56m-330m depth levels. Presented as current speed (a), zonal currents (b), and meridional currents (c).

Anomalously warm water parcels that enter the EUC in the West Pacific are rapidly advected eastward, shoaling nearly 100m along isopycnals in transit (Fig. 11). Some of this heat has reached the East Pacific by November (Fig. 11b). This transport continues through the winter (Fig. 11c), with a significant warming of tropical East Pacific thermocline waters being achieved by May (Fig. 11d). Little anomalous heat remains in the equatorial West Pacific by the start of the following storm season. Rapid relocation of OHU via the West Pacific subtropical cell, Mindanao Current, and Equatorial Undercurrent serves to explain the low persistence of OHU in the West Pacific and provides for a connection between typhoon activity and warming of East Pacific tropical thermocline waters on interseasonal timescales.

4. DISCUSSION

The interaction of tropical cyclones with the ocean produces a non-negligible heating of the thermocline with potential implications for the ocean climate system. Though a global phenomena, viewing the impact of tropical cyclones (TCs) on the ocean on a regional basis sheds light on the physical mechanisms driving the generation and redistribution of TC induced Ocean Heat Uptake (OHU). Our estimates of global heat uptake magnitude and rates are consistent with the results of recent observational and modeling studies. We find that TC induced heat uptake can augment the basin heat content by up to 10% of the local seasonal variability in those basins with the greatest storm activity.

Due to the single year of model integration and analysis, we are unable to address questions related to the poleward export of anomalous heating through the Atlantic meridional overturning circulation predicted by Emanuel (2001). Rather, our analysis identifies a rapid equatorial convergence of heat through the shallower and more rapid wind driven West Pacific subtropical cell, taking place concurrently and on shorter timescales.

The pumping of heat into the tropical Pacific thermocline suggests possible ventilation by the El Niño-Southern Oscillation (ENSO), allowing the ocean to remain in thermodynamic balance. More complex interactions with ENSO are also possible with changes to the equatorial thermocline structure (Fedorov et al, 2010). Results from our study are subject to uncertainties associated with model formulation (e.g., parameterizations) and grid resolution. We therefore recommend further examinations in global eddying simulations of the mechanisms for TC induced heat transport and quantitative estimates of OHU.

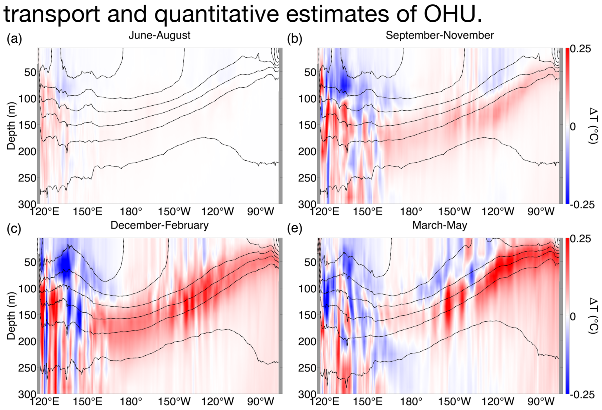

Fig. 11: temperature anomalies averaged from 5°S-5°N in the Pacific Equatorial Undercurrent, with average isopycnals from the same period superimposed, for (a) June, July, August; (b) September, October, November; (c) December, January, February; and (d) March, April, May.

5. REFERENCES

Bender, M. A., I. Ginis, R. Tuleya, B. Thomas, and T. Marchok, 2007: The Operational GFDL Coupled Hurricane-Ocean Prediction System and a Summary of its Performance. *Mon. Wea. Rev.*, **135 (12)**, 3965-3989.

Cheng, L., J. Zhu, and R. L. Sriver, In review: Global Representation of Tropical Cyclone-Induced Thermal Changes Using Argo Data, Part I: Methods and Results. *J. Climate*, 1-40

Delworth, T. L., et al., 2012: Simulated Climate Change in the GFDL CM2.5 High-Resolution Coupled Climate Model. *J. Climate*, **25 (8)**, 2755-2781.

Emanuel, K. A., 2001: Contribution of Tropical Cyclones to Meridional Heat Transport by the Oceans. *J. Geophys. Research*, **106 (D14)**, 14771-14781.

Fedorov, A. V., C. M. Brierley, and K. A. Emanuel, 2010: Tropical Cyclones and Permanent El Niño in the Early Pliocene Epoch. *Nature*, **463 (7248)**, 1066-1070.

Fox-Kemper, B., et al., 2011: Parameterization of Mixed Layer Eddies. III: Implementation and Impact in Global Ocean Climate Simulations. *Ocean Model.*, **39 (1-2)**, 61-78.

Griffies, S. M., 2009: Elements of MOM4p1. *GFDL Ocean Group Tech. Rep.*, **6**, 444.

Griffies, S. M., et al., 2009: Coordinated Ocean-Ice Reference Experiments (COREs). *Ocean Model.*, **26 (1-2)**, 1-46.

Holland, G. J., 1980: An Analytic Model of the Wind and Pressure Profiles in Hurricanes. *Mon. Wea. Rev.*, **108 (8)**, 1212-1218.

Jansen, M. F. and R. Ferrari, 2009: Impact of Latitudinal Distribution of Tropical Cyclones on Ocean Heat Transport. *Geophys. Res. Lett.*, **37 (3)**, L03 602.

Jansen, M. F., R. Ferrari, and T. A. Mooring, 2010: Seasonal Versus Permanent Thermocline Warming by Tropical Cyclones. *Geophys Res. Lett.*, **37 (3)**, L03 602.

Kaufman, M., I. Ginis, R. M. Yablonsky, and B. Thomas, In prep: Evaluating Ocean Model Resolution Under Hurricane Conditions. *Mon. Wea. Rev.*

Large, W. G., J. C. McWilliams, and S. C. Doney, 1994: Ocean Vertical Mixing: A Review and a Model with a Nonlocal Boundary Layer Parameterization. *Rev. Geophys.*, **32 (4)**, 363-403.

Large, W. G. and S. G. Yeager, 2004: Diurnal to Decadal Global Forcing for Ocean and Sea-Ice Models: The Data Set and Flux Climatologies. *NCAR Technical Note*.

Manucharyan, G. E., C. M. Brierley, and A. V. Fedorov , 2011: Climate Impacts of Intermittent Upper Ocean Mixing Induced by Tropical Cyclones. *J. Geophys. Res.*, **116 (C11)**, C11 038.

McCreary Jr., J. P. and P. Lu, 1994: Interaction Between the Subtropical and Equatorial Ocean Circulations: The Subtropical Cell. *J. Phys. Oceanogr.*, **24**, 466-497.

Moon, I.-J., I. Ginis, T. Hara, and B. Thomas, 2007: A Physics-Based Parameterization of Air-Sea Momentum Flux at High Wind Speeds and its Impact on Hurricane Intensity Predictions. *Mon. Wea. Rev.*, **135 (8)**, 2869-2878.

Price, J. F., 1981: Upper Ocean Response to a Hurricane. *J. Phys. Oceanogr.*, **11 (2)**, 153-175.

Qu, T. and R. Lukas, 2003: The Bifurcation of the North Equatorial Current in the Pacific*. *J. Phys. Oceanogr.*, **33 (1)**, 5-18.

Zhang, S., M. J. Harrison, A. Rosati, and A. Wittenberg, 2007: System Design and Evaluation of Coupled Ensemble Data Assimilation for Global Oceanic Climate Studies. *Mon. Wea. Rev.*, **135 (10)**, 3541-3564.